Icarus 450 (2026) 116975

Contents lists available at ScienceDirect

Icarus

journal homepage: www.elsevier.com/locate/icarus

Note

The effect of thermo-tidal winds on the expansion of local and regional dust storms on Mars

Anthony D. Toigo [a,*], Mark I. Richardson [b], Huiqun Wang [c]

[a] Johns Hopkins University Applied Physics Laboratory, USA
[b] Aeolis Research, USA
[c] Smithsonian Astrophysical Observatory, Harvard-Smithsonian Center for Astrophysics, USA

A B S T R A C T

Recent imaging observations from the Emirates Exploration Imager show significant diurnal variation of dust storm evolution that is unresolved by traditional daily global mapping from sun synchronous orbit. Motivated by these observations, we present initial simulations from a global numerical model examining the diurnal evolution of transported, radiatively active dust from simulated dust sources. The simulations show that the expansion and mixing of large local and regional dust storms are strongly modified by the wide diurnal "reach" of thermo-tidal winds. In particular, thermo-tidal winds can rapidly spread dust between adjacent storms and can translate storms over significant distances, including transporting storm dust between different meteorological regimes.

1. Introduction

The mechanisms involved in the evolution of dust storms along the size spectrum from local lifting events to global storms remains one of the primary unsolved problems of Martian meteorology and climate dynamics (Kahre et al., 2017). The increase in the strength and extent of the Hadley circulation during the final transition to a global storm has long been recognized, and the feedback between widespread atmospheric dust, increased atmospheric heating, enhanced circulation, and increasingly widespread dust mixing has been noted as the important final growth mechanism (Haberle et al., 1982; Murphy et al., 1993; Murphy et al., 1995; Wilson, 1997; Newman et al., 2002a; Basu et al., 2006; Newman and Richardson, 2015; Bertrand et al., 2020). Earlier-stage growth mechanisms are less clear, with the most documented, specific dynamical mechanism probably being the extratropical synoptic eddy and Hadley circulation coupling via the thermo-tidal "gate" (Wang et al., 2003; Wang et al., 2005).

Much modeling emphasis to date has been on trying to capture the observed size spectrum of storms (Newman et al., 2002a; Basu et al., 2004; Kahre et al., 2006; Hollingsworth and Kahre, 2010; Newman and Richardson, 2015; Newman et al., 2019), trying to match different aspects of observations (e.g., ground and air heating, thermo-tidal responses, dust vertical distribution) (Bertrand et al., 2020; Wu et al., 2020; Batterson et al., 2023; Li et al., 2025), or to simulate the multi-annual dust cycle (Newman et al., 2002a; Basu et al., 2004; Kahre et al., 2006; Newman and Richardson, 2015; Kahre et al., 2017; Newman et al., 2019; Bertrand et al., 2020).

Observationally, a long-term catalog of storm development has been compiled using Mars Daily Global Maps created from images (Wang, 2007; Wang et al., 2011; Wang and Richardson, 2015; Wang, 2017; Wang, 2018; Wang et al., 2020; Battalio and Wang, 2021; Battalio et al., 2023; Wang et al., 2023a; Wang et al., 2023b) from the Mars Global Surveyor (MGS) Mars Orbiter Camera (MOC) (Cantor et al., 2002) and the Mars Reconnaissance Orbiter (MRO) Mars Color Imager (MARCI) (Malin et al., 2001), both at approximately fixed local times. Despite the wealth of imaging data and commensurate observations in the thermal infrared (Smith, 2004; Montabone et al., 2015; Kass et al., 2016; Smith, 2019; Kass et al., 2020; Kleinböhl et al., 2020; Kleinböhl et al., 2024), the specifics of storm growth from small storms to large regional storms has remained problematic and relatively under-explored (Toigo et al., 2018).

As will be discussed below, part of the problem of grappling with storm growth at these scales has been the lack of constraints from diurnally resolved imaging of the atmosphere. This has been greatly facilitated by the Emirates Mars Mission (EMM) Emirates Exploration Imager (EXI) instrument, where the elliptical orbit allows regions of the planet to be imaged multiple times a day (Jones, 2021; Amiri et al., 2022). These images allow observation of the evolution of dust storms over a single sol, showing significant lateral displacement and some diffusion of the storms (Guha et al., 2024). This is in contrast with the traditional dust storm climatologies from daily fixed MDGMs (Wang and Ingersoll, 2002; Wang and Richardson, 2015; Battalio and Wang, 2021; Battalio et al., 2023; Wang et al., 2023b), which unavoidably miss this significant diurnal evolution. Although other missions (MAVEN, TGO,

* Corresponding author.

https://doi.org/10.1016/j.icarus.2026.116975
Received 30 December 2025; Received in revised form 17 January 2026; Accepted 26 January 2026
Available online 29 January 2026

MEX, etc.) also took images at various local times (Hernandez-Bernal, 2024; McClintock, 2015; Thomas, 2017), the EMM/EXI images have readily available geolocation and other information for each pixel, frequent local time sampling, and wide spatial coverage, which are more suitable for our study (see Data Availability).

Motivated by the EXI images, this paper examines the diurnal evolution of dust storms using a global circulation model (GCM) with radiatively and dynamically interactive dust (Newman and Richardson, 2015; Newman et al., 2019). We seed the storms using prescribed surface dust emission, and we separately track the dust associated with each storm and the background opacity. This new approach makes it possible to attribute dust variations to different sources and to illustrate the diurnal effect on storm evolution.

2. Modeling with interactive dust

This study uses the MarsWRF GCM (Richardson et al., 2007; Toigo et al., 2012). MarsWRF treats atmospheric radiative transfer due to CO_2 gas, absorption, emission and scattering due to dust (Mischna et al., 2012), boundary layer and free atmosphere eddy mixing (Hong et al., 2006), ground temperature evolution using a 15-layer scheme, and the CO_2 cycle (Guo et al., 2009). The model has an Eulerian Mass dynamical core, which discretizes the atmosphere on a structured C-grid horizontally, and a terrain-following, pressure-based eta grid vertically (Powers et al., 2017). In this study, we use the model with a $2^\circ \times 2^\circ$ horizontal mesh and 52 layers between the surface and roughly 120 km (Li et al., 2025).

MarsWRF includes a fully interactive dust cycle scheme (Newman and Richardson, 2015; Newman et al., 2019), with parameterized lifting mechanisms related to resolved winds and unresolved convective processes, dust sedimentation, and surface dust availability. Dust is tracked as a tracer that is advected and mixed by the resolved winds and parameterized diffusion. The abundance of dust in each grid cell is used to calculate the optical depth in the radiative transfer scheme.

For dust injection, in addition to physically motivated dust lifting mechanisms (Newman et al., 2002b), the model can augment dust lifting based upon the offset between the simulated and a target dust optical depth ("nudging"). In this study, we use nudging instead of the physically motivated injection schemes. The target for tracking can be the Montabone et al. (2015) observational-based climatology, or any other gridded, time-evolving climatology. The tracking scheme employs a dust lifting rate, L_o (kg/m^{2}s) defined as:

$$L_o = \frac{C \times (\tau_{obs} - \tau_{model})}{t_{adj}} \quad (1)$$

where C relates the dust column mass density to the optical depth at the reference wavelength and will vary depending upon model spectral resolution, dust particle size distribution, and dust optical properties used (for the cases in this study, C=1.096×10^{-3} kg/m^2), τ_{obs}-τ_{model} is the optical depth offset, and t_{adj} is an adjustable timescale (set to 2 sols for the background optical depth and 0.25 sols for the imposed storms).

For this study, we use this dust optical depth “nudging” (Eq. 1) in two ways: 1) we use it to track the Mars Year (MY) 30 Montabone et al. (2015) dust climatology (without activation of physical dust lifting mechanisms); and 2) we use it to impose idealized storm areas for limited periods during simulations. Note that MY 30 (corresponding to late 2009 to late 2011) is chosen as it provides a relatively dust-storm-free background opacity (Kleinböhl et al., 2024) as compared with other years. Imposed storms are defined as simple rectilinear longitude – latitude areas (Fig. 1a and b), similar to the imposition of dust opacity by Toigo et al. (2018). We apply the storm forcing for 5° of L_s starting at L_s = 210°.

Dust from each of the different sources is tracked separately and thus three separate global inventories of atmospheric and surface dust are tracked in this study. When two or more non-zero L_o rates are calculated for a given model grid point, only the largest one is used, and the others are set to zero. For the radiative calculations, it is possible to use any combination of the prognostic dust amounts to derive optical depth. In these experiments, we sum the dust amounts from all active dust arrays for each model grid box.

3. Diurnal transport and mixing of dust

To explore the influence of diurnal winds on regional-scale storms, we imposed storms by activating lifting in Chryse Planitia and in the region between Argyre and south of Valles Marineris. The dust lifting rates for each storm were set to generate a 0.67 μm optical depth of 3 in 6 Mars hours. The evolution of these two storms every 6 Mars hours over the subsequent three Mars sols are shown in the left two columns of Fig. 1. The evolution of the total 0.67 μm optical depth (including the MY30 background) is shown in the third column, and the mass-weighted average wind in the lowest 600 m is shown in the fourth column. A video of the output at 5 minute sampling over multiple sols is available online (see Data Availability).

Despite lifting remaining fixed to the areas where the storms are prescribed (shown in Fig. 1a and b), the area of significant dust mass and optical depth spreads rapidly due to the flow at both locations (e.g., compare Fig. 1a and m 24 h apart). Although at any point in the flow the thermo-tidal winds rotate over 24 h, on the scale of the imposed storms, the rotating wind field is non-uniform. As a result, the storm does not simply translate around a circuit but is sheared and stretched. Within just one sol, and without any increase in lifting area, the storm area (defined as anywhere that has at least 10% of the peak storm dust column mass) has doubled due to this shearing and stretching. Comparing Storm 1 and Storm 2, the nature of the spreading is different. For example, Storm 1 (first column of Fig. 1) shows more north-south elongation, while Storm 2 (second column of Fig. 1) expands in a more east-west direction. This suggests that the details of the thermo-tidal diurnal wind field matter greatly in how a storm at a given location will expand (see also the fourth column of Fig. 1 and the videos referenced in the Data Availability).

The second and third sol of the imposed storm in the northern hemisphere highlights another significant effect of the thermal tides. The northern extent of the northern storm becomes pulled into the northern autumnal baroclinic storm track (Hollingsworth et al., 1996; Hollingsworth and Kahre, 2010) and the dust becomes entrained in a curved front (Wang et al., 2003; Wang and Fisher, 2009). In this way, tidal dislocation of the dust storm has caused some dust to transfer from a sub-tropical location into a high-latitude extra-tropical dynamical system. The southern storm stays within the developing southern summer monsoonal mode of the Hadley circulation, but even over 3 sols it can been seen to spread out in the southern component of the Hadley cell flow.

4. Summary, discussion, and further work

The significance of thermal tides for the general circulation has been emphasized in the works of Zurek (Zurek, 1976; Leovy and Zurek, 1979; Zurek and Leovy, 1981; Zurek, 1986; Zurek and Haberle, 1988) and Wilson and Hamilton (1996). As the connector in the “tidal gate” mechanism of baroclinic frontal storm “flushing,” their influence on Martian meteorology has also been underscored (Wang et al., 2003; Wang et al., 2005). However, the initial results presented here suggest that thermo-tidal motions may be far more generally important for moderate-sized storm growth than recognized to date.

We refer to the daily varying winds generally as thermo-tidal motions here, but near the surface, such winds likely will have contributions due to slope-related and sea-breeze flows (see Richardson and Newman (2018) for an extended discussion). In some discussions, these typically mesoscale diurnal circulations are folded into the category of "tidal" motions, but even if we limit the term "tide" to be strictly the

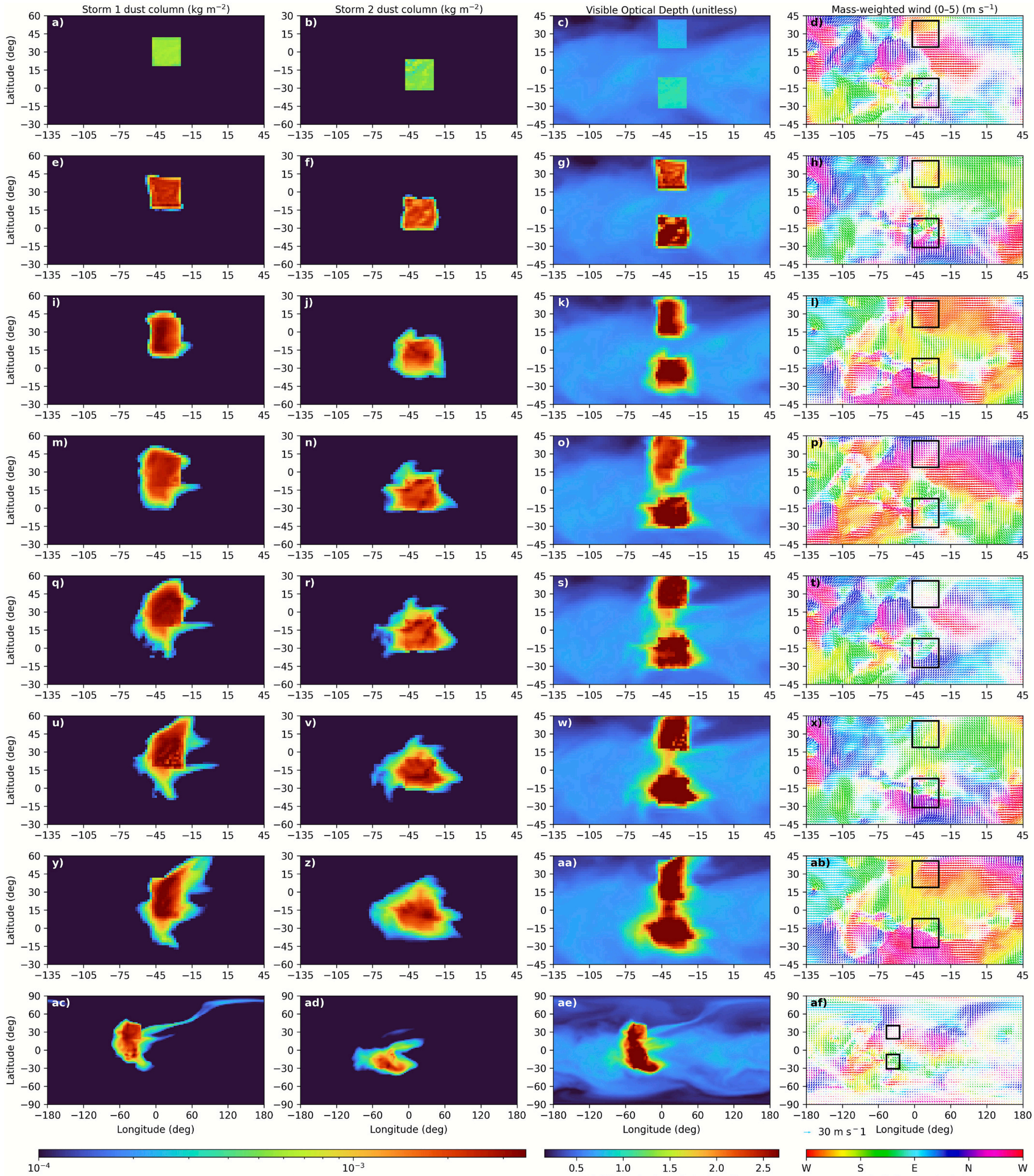

Fig. 1. The evolution of two simulated storms forced by dust injection in the square areas indicated in the top row, starting at $L_S = 210^{\circ}$. Left two columns show the total column dust (kg/m2) distribution for Storm 1 (first column) and Storm 2 (second column) every 6 h for 36 h (1.5 Mars sols), with the last row (ac,ad) being 3 sols after the storm started. Note the difference in latitude-longitude coverage of the individual panels. The third column shows the total visible (0.67 μm) dust optical depth due to the storms and the Montabone et al. (2015) MY30 climatology background at the corresponding timesteps. The fourth column shows the wind vectors (as arrows where the lengths and colors indicate speeds and directions, respectively) in the lowest 600 m of the atmosphere, highlighting the significant diurnal cycle. (For interpretation of the references to color in this figure legend, the reader is referred to the web version of this article.)

global normal modes, the diurnal variations at the bottom boundary are an important part of tidal forcing. However, simulations run with no topography or thermal property variations (figure and videos are available online, see Data Availability) show qualitatively similar storm translation and distortion as in Fig. 1. As such, it is reasonable to think of the agitation as being fundamentally tidal in nature, albeit recognizing that real surface properties complicate the tidal flows.

In idealized experiments, Toigo et al. (2018) examined the distal influence of geographically fixed local and regional sized storms on adjacent regions. However, Fig. 1 shows that the most rapid communication of "information" about a given storm to adjacent regions is likely tidal advection of storm dust to those adjacent regions. Toigo et al. (2018) were specifically looking for dynamical mechanisms that might allow storms to grow through their own intrinsic radiative-dynamical feedback on the atmosphere (via excited waves and induced circulations). Indeed, such mechanisms may be significant under certain conditions, but our initial results suggest that thermo-tidal "agitation" of the atmosphere may provide a much more rapid means of storm growth individually and through merging once storms get to the relevant scales and configurations.

The role of tides, as indicated here are at least two-fold: 1) they facilitate generation of stretching and shearing of storms that provide a mechanism for storm expansion, 2) they translate storms across meteorological system boundaries (e.g., a generalized version of the "tidal gate" mechanism). Further, since the tidal winds also translate storms over regions where dust lifting was not previously ongoing, it seems plausible that they might induce dust-lifting winds over areas amenable to dust lifting that would not otherwise have become involved in a given storm.

While encouraging, further work is needed to examine how the rates of shearing, spread, and the radius of influence due to thermo-tidal effects vary as a function of location and season, and the relative importance of these effects as compared to more local mechanisms induced at the storm edges. This will provide a better idea of when, where, and how thermal tides impact storm growth, helping to fill a critical gap in current understanding of Martian dust storms.

CRediT authorship contribution statement

Anthony D. Toigo: Writing – review & editing, Writing – original draft, Software, Methodology, Investigation, Conceptualization. **Mark I. Richardson:** Writing – review & editing, Writing – original draft, Visualization, Software, Methodology, Investigation, Formal analysis, Data curation, Conceptualization. **Huiqun Wang:** Writing – review & editing, Writing – original draft, Project administration, Investigation, Funding acquisition, Formal analysis, Conceptualization.

Declaration of competing interest

The authors declare that they have no known competing financial interests or personal relationships that could have appeared to influence the work reported in this paper.

Acknowledgements

We acknowledge the support of NASA Solar System Workings Program grant #80NSSC21K1831 for the work described here. Resources supporting this work were provided by the NASA High-End Computing (HEC) Program through the NASA Advanced Supercomputing (NAS) Division at Ames Research Center. WRF is developed and supported by the National Center for Atmospheric Research (NCAR).

Data availability

Data will be made available on request. Supplemental figures and movies are available through the Zenodo data repository at doi:10.5281/zenodo.18252821.

References

Amiri, H., et al., 2022. The emirates Mars mission. Space Sci. Rev. 218, 4.

Basu, S., Richardson, M.I., Wilson, R.J., 2004. Simulation of the Martian dust cycle with the GFDL Mars GCM. J. Geophys. Res.: Planets. 109.

Basu, S., Wilson, J., Richardson, M., Ingersoll, A., 2006. Simulation of spontaneous and variable global dust storms with the GFDL Mars GCM. J. Geophys. Res.: Planets. 111.

Battalio, J.M., Wang, H., Richardson, M.I., Toigo, A.D., Saidel, M., 2023. Spatial extent of dust storm boundaries in the Mars dust activity database. Icarus 400, 115567.

Battalio, M., Wang, H., 2021. The Mars dust activity database (MDAD): a comprehensive statistical study of dust storm sequences. Icarus 354, 114059.

Batterson, C.M., Kahre, M.A., Bridger, A.F., Wilson, R.J., Urata, R.A., Bertrand, T., 2023. Modeling the "B" regional dust storm on Mars: dust lofting mechanisms predicted by the new NASA Ames Mars GCM. Icarus 400, 115542.

Bertrand, T., Wilson, R.J., Kahre, M.A., Urata, R., Kling, A., 2020. Simulation of the 2018 global dust storm on Mars using the NASA Ames Mars GCM: a multitracer approach. J. Geophys. Res.: Planets. 125, e2019JE006122.

Cantor, B., Malin, M., Edgett, K.S., 2002. Multiyear Mars orbiter camera (MOC) observations of repeated Martian weather phenomena during the northern summer season. J. Geophys. Res.: Planets. 107, 3–1–3–8.

Guha, B.K., Gebhardt, C., Young, R.M., Wolff, M.J., Montabone, L., 2024. Seasonal and diurnal variations of dust storms in Martian year 36 based on the EMM-EXI database. J. Geophys. Res.: Planets. 129, e2023JE008156.

Guo, X., Lawson, W.G., Richardson, M.I., Toigo, A., 2009. Fitting the Viking lander surface pressure cycle with a Mars general circulation model. J. Geophys. Res.: Planets. 114.

Haberle, R.M., Leovy, C.B., Pollack, J.B., 1982. Some effects of global dust storms on the atmospheric circulation of Mars. Icarus 50, 322–367.

Hollingsworth, J., Kahre, M., 2010. Extratropical cyclones, frontal waves, and Mars dust: modeling and considerations. Geophys. Res. Lett. 37.

Hernandez-Bernal, J., et al., 2024. The visual monitoring camera (VMC) on Mars express: A new science instrument made from an old webcam orbiting Mars. Planet. Space Sci. 251, 105972.

Hollingsworth, J.L., et al., 1996. Orographic control of storm zones on Mars. Nature 380, 413–416.

Hong, S.-Y., Noh, Y., Dudhia, J., 2006. A new vertical diffusion package with an explicit treatment of entrainment processes. Mon. Weather Rev. 134, 2318–2341.

Jones, A., et al., 2021. The emirates exploration imager (EXI) instrument on the emirates Mars mission (EMM) hope mission. Space Sci. Rev. 217, 81.

Kahre, M.A., Murphy, J.R., Haberle, R.M., 2006. Modeling the Martian dust cycle and surface dust reservoirs with the NASA Ames general circulation model. J. Geophys. Res.: Planets. 111.

Kahre, M.A., et al., 2017. The Mars dust cycle. In: The atmosphere and climate of Mars, 18, p. 295.

Kass, D., Kleinböhl, A., McCleese, D., Schofield, J., Smith, M., 2016. Interannual similarity in the Martian atmosphere during the dust storm season. Geophys. Res. Lett. 43, 6111–6118.

Kass, D., et al., 2020. Mars climate sounder observation of Mars' 2018 global dust storm. Geophys. Res. Lett. 47, e2019GL083931.

Kleinböhl, A., et al., 2020. Diurnal variations of dust during the 2018 global dust storm observed by the Mars climate sounder. J. Geophys. Res. Planets 125, e2019JE006115.

Kleinböhl, A., et al., 2024. Far infrared radiative properties of Mars atmospheric aerosols and their application to Mars climate sounder retrievals of aerosol profiles, aerosol columns and surface temperatures. Icarus 419, 116000.

Leovy, C.B., Zurek, R.W., 1979. Thermal tides and Martian dust storms: direct evidence for coupling. J. Geophys. Res. Solid Earth 84, 2956–2968.

Li, L., et al., 2025. Impacts of dry deposition processes with resolved dust particle sizes on simulating the Martian dust. J. Geophys. Res. Planets 130, e2024JE008616.

Malin, M., et al., 2001. Mars color imager (MARCI) on the Mars climate orbiter. J. Geophys. Res. Planets 106, 17651–17672.

McClintock, W.E., et al., 2015. The imaging ultraviolet spectrograph (IUVS) for the MAVEN mission. Space Sci. Rev. 195, 75–124.

Mischna, M.A., Lee, C., Richardson, M., 2012. Development of a fast, accurate radiative transfer model for the Martian atmosphere, past and present. J. Geophys. Res.: Planets. 117.

Montabone, L., et al., 2015. Eight-year climatology of dust optical depth on Mars. Icarus 251, 65–95.

Murphy, J.R., Haberle, R.M., Toon, O.B., Pollack, J.B., 1993. Martian global dust storms: zonally symmetric numerical simulations including size-dependent particle transport. J. Geophys. Res.: Planets. 98, 3197–3220.

Murphy, J.R., Pollack, J.B., Haberle, R.M., Leovy, C.B., Toon, O.B., Schaeffer, J., 1995. Three-dimensional numerical simulation of Martian global dust storms. J. Geophys. Res.: Planets. 100, 26357–26376.

Newman, C.E., Richardson, M.I., 2015. The impact of surface dust source exhaustion on the Martian dust cycle, dust storms and interannual variability, as simulated by the MarsWRF general circulation model. Icarus 257, 47–87.

Newman, C.E., Lewis, S.R., Read, P.L., Forget, F., 2002a. Modeling the Martian dust cycle 2. Multiannual radiatively active dust transport simulations. J. Geophys. Res.: Planets. 107, 7–1–7–15.

Newman, C.E., Lewis, S.R., Read, P.L., Forget, F., 2002b. Modeling the Martian dust cycle, 1. Representations of dust transport processes. J. Geophys. Res.: Planets. 107, 6–1–6–18.

Newman, C.E., Lee, C., Mischna, M.A., Richardson, M.I., Shirley, J.H., 2019. An initial assessment of the impact of postulated orbit-spin coupling on Mars dust storm variability in fully interactive dust simulations. Icarus 317, 649–668.
Powers, J.G., et al., 2017. The weather research and forecasting model: overview, system efforts, and future directions. Bull. Am. Meteorol. Soc. 98, 1717–1737.
Richardson, M.I., Newman, C.E., 2018. On the relationship between surface pressure, terrain elevation, and air temperature. Part I: The large diurnal surface pressure range at Gale Crater, Mars and its origin due to lateral hydrostatic adjustment. Planet. Space Sci. 164, 132–157.
Richardson, M.I., Toigo, A.D., Newman, C.E., 2007. PlanetWRF: a general purpose, local to global numerical model for planetary atmospheric and climate dynamics. J. Geophys. Res.: Planets. 112.
Smith, M.D., 2004. Interannual variability in TES atmospheric observations of Mars during 1999–2003. Icarus 167, 148–165.
Smith, M.D., 2019. THEMIS observations of the 2018 Mars global dust storm. J. Geophys. Res.: Planets. 124, 2929–2944.
Thomas, N., et al., 2017. The colour and stereo surface imaging system (CaSSIS) for the ExoMars trace gas orbiter. Space Sci. Rev. 212, 1897–1944.
Toigo, A.D., Lee, C., Newman, C.E., Richardson, M.I., 2012. The impact of resolution on the dynamics of the martian global atmosphere: varying resolution studies with the MarsWRF GCM. Icarus 221, 276–288.
Toigo, A.D., Richardson, M.I., Wang, H., Guzewich, S.D., Newman, C.E., 2018. The cascade from local to global dust storms on Mars: temporal and spatial thresholds on thermal and dynamical feedback. Icarus 302, 514–536.
Wang, H., 2007. Dust storms originating in the northern hemisphere during the third mapping year of Mars global surveyor. Icarus 189, 325–343.
Wang, H., 2017. Major dust storms and westward traveling waves on Mars. Geophys. Res. Lett. 44, 3493–3501.
Wang, H., 2018. Cross-equatorial Flushing dust storms and northern hemisphere transient eddies: an analysis for Mars year 24. J. Geophys. Res.: Planets. 123, 1732–1745.
Wang, H., Fisher, J.A., 2009. North polar frontal clouds and dust storms on Mars during spring and summer. Icarus 204, 103–113.
Wang, H., Ingersoll, A.P., 2002. Martian clouds observed by Mars global surveyor Mars orbiter camera. J. Geophys. Res.: Planets. 107, 8–1–8–16.
Wang, H., Richardson, M.I., 2015. The origin, evolution, and trajectory of large dust storms on Mars during Mars years 24–30 (1999–2011). Icarus 251, 112–127.
Wang, H., Richardson, M.I., Wilson, R.J., Ingersoll, A.P., Toigo, A.D., Zurek, R.W., 2003. Cyclones, tides, and the origin of a cross-equatorial dust storm on Mars. Geophys. Res. Lett. 30.
Wang, H., Zurek, R.W., Richardson, M.I., 2005. Relationship between frontal dust storms and transient eddy activity in the northern hemisphere of Mars as observed by Mars global surveyor. J. Geophys. Res.: Planets. 110.
Wang, H., Toigo, A.D., Richardson, M.I., 2011. Curvilinear features in the southern hemisphere observed by Mars global surveyor Mars orbiter camera. Icarus 215, 242–252.
Wang, H., Battalio, M., Huber, Z., 2023a. MRO MARCI Mars Daily Global Maps pds. 175.
Wang, H., Saidel, M., Richardson, M.I., Toigo, A.D., Battalio, J.M., 2023b. Martian dust storm distribution and annual cycle from Mars daily global map observations. Icarus 394, 115416.
Wang, H.H., Battalio, M., Huber, Z., 2020. MRO MARCI Mars daily global maps V2. Harvard Dataverse dataset, p. 462.
Wilson, R.J., 1997. A general circulation model simulation of the Martian polar warming. Geophys. Res. Lett. 24, 123–126.
Wilson, R.J., Hamilton, K., 1996. Comprehensive model simulation of thermal tides in the Martian atmosphere. J. Atmos. Sci. 53, 1290–1326.
Wu, Z., Li, T., Zhang, X., Li, J., Cui, J., 2020. Dust tides and rapid meridional motions in the Martian atmosphere during major dust storms. Nat. Commun. 11, 614.
Zurek, R., Leovy, C., 1981. Thermal tides in the dusty Martian atmosphere: a verification of theory. Science 213, 437–439.
Zurek, R.W., 1976. Diurnal tide in the Martian atmosphere. J. Atmos. Sci. 33, 321–337.
Zurek, R.W., 1986. Atmospheric tidal forcing of the zonal-mean circulation: the Martian dusty atmosphere. J. Atmos. Sci. 43, 652–670.
Zurek, R.W., Haberle, R.M., 1988. Zonally symmetric response to atmospheric tidal forcing in the dusty Martian atmosphere. J. Atmos. Sci. 45, 2469–2485.